

# Chemical evolution using SPH cosmological simulations. I: implementation, tests and first results

M. B. Mosconi<sup>1</sup>, P. B. Tissera<sup>2,3</sup>, D. G. Lambas<sup>1,3</sup>, S. A. Cora<sup>3,4</sup>

<sup>1</sup> *Grupo I.A.T.E., Observatorio Astronómico de Córdoba, Argentina.*

<sup>2</sup> *Instituto de Astronomía y Física del Espacio, Casilla de Correos 67, Suc. 28, Buenos Aires (1428), Argentina.*

<sup>3</sup> *Consejo Nacional de Investigaciones Científicas y Técnicas, Argentina.*

<sup>4</sup> *Observatorio Astronómico de La Plata, U.N.L.P., Argentina.*

Accepted ..... Received .....; in original form .....

## ABSTRACT

We develop a model to implement metal enrichment in a cosmological context based on the hydrodynamical AP3MSPH code described by Tissera, Lambas and Abadi (1997). The star formation model is based on the Schmidt law and has been modified in order to describe the transformation of gas into stars in more detail. The enrichment of the interstellar medium due to supernovae I and II explosions is taken into account by assuming a Salpeter Initial Mass Function and different nucleosynthesis models. The different chemical elements are mixed within the gaseous medium according to the Smooth Particle Hydrodynamics technique. Gas particles can be enriched by different neighbouring particles at the same time. We present tests of the code that assess the effects of resolution and model parameters on the results. We show that the main effect of low numerical resolution is to produce a more effective mixing of elements, resulting in abundance relations with less dispersion. We have performed cosmological simulations in a standard Cold Dark Matter scenario and we present results of the analysis of the star formation and chemical properties of the interstellar medium and stellar population of the simulated galactic objects. We show that these systems reproduce abundance ratios for primary and secondary elements of the interstellar medium, and the correlation between the (O/H) abundance and the gas fraction of galaxies. We find that star formation efficiency, the relative rate of supernovae II to supernovae I and life-time of binary systems as well as the stellar nucleosynthesis model adopted affect the chemical properties of baryons. We have compared the results of the simulations with an implementation of the one-zone Simple Model, finding significant differences in the global metallicities of the stars and gas as well as their correlations with dynamical parameters of the systems. The numerical simulations performed provide a detailed description of the chemical properties of galactic objects formed in hierarchical clustering scenarios and proved to be useful tools to deepen our understanding of galaxy formation and evolution.

**Key words:** cosmology: theory - galaxies: formation - galaxies: evolution - galaxies: abundances.

## 1 INTRODUCTION

In recent years, our knowledge of the high redshift Universe has increased dramatically allowing us to start constructing a picture of how the different morphological types evolve (e.g. Steidel and Hamilton 1992; Madau 1995; Lilly et al. 1995; Cowie et al. 1996; Ellis et al. 1996; Steidel et al. 1998). In particular, the comoving star formation history first depicted by Madau et al. (1996) has resulted in a very useful way of quantifying galaxy evolution, under certain hypothesis. Since star formation directly translates into metal en-

richment of the interstellar medium (ISM), observations of these two processes help astronomers to constrain models of the formation of the structure. In particular, Lyman alpha forests, damped Lyman alpha systems and Lyman alpha break galaxies have all contributed to estimate the cosmic metal ejection and star formation rates (e.g., Lu et al. 1996; Pettini et al. 1997). However, we are still far from drawing a consistent picture since several points remain to be clarified. In this respect, the integration of the dust corrected cosmic star formation history of the Universe up to  $z = 0$

can account for the entire stellar mass content in spirals and spheroids at present times. However, when we look at the metal content at  $z \simeq 2.5$ , only 10% of what is expected is actually measured (Renzini 1998). Regarding the chemical properties of galaxies, most of the available observations are restricted to the Galaxy, and in particular, to the solar neighbourhood (e.g., Edvardsson et al. 1993; Gratton et al. 1996; Rocha-Pinto et al. 2000). Extragalactic observations of HII regions provide information on the chemical content in other galaxies (e.g., Pagel 1992; Garnett et al. 1995; Kennicutt and Garnett 1996; Kobulnicky and Skillman 1996).

Chemical evolution models are a useful tool to attempt to study the physical processes that might determine the chemical characteristics of the different galaxies. Detailed modelling can be found in studies of the Galaxy (e.g., Ferrini et al. 1992; Tossi 1996; Chiappini, Matteucci and Gratton 1997 and references therein). These analytical models carefully treat stellar evolution. However, they cannot account for dynamical evolution, and certainly, not for hierarchical clustering. From a numerical point of view, metallicity enrichment mechanisms have been implemented in hydrodynamical simulations in different ways. The first attempts were done by Larson (1975, 1976). Other implementations came after using diverse techniques such as chemodynamical models (e.g., Burkert et al. 1992; Samland et al. 1997) which describe in more detail the interstellar medium evolution. On the other hand, this approach uses a very simple prescription for galaxy formation where the dark matter halo is either not considered at all or assumed to be static. However, there are strong evidences from observations of normal spirals that the dark matter is dynamically important within the luminous radius (e.g., Bottema 1992; Courteau, de Jong & Broeils 1996; Rhee 1996), and that the response of the dark matter to the presence of baryons affect their evolution (Blumenthal et al. 1996; Tissera & Domínguez-Tenreiro 1998) and, as a consequence, the star formation process (Mihos & Hernquist 1996; Barnes & Hernquist 1996; Tissera 2000; Navarro & Steinmetz 2000). A first approach to include chemical evolution in Smooth Particle Hydrodynamical (SPH) code is described by Steinmetz and Müller (1994, 1995) followed by Raiteri, Villata and Navarro (1996). These works run prepared-cosmological initial conditions where the formation and evolution of only one object was studied. These models have shed light on some physical mechanisms that may control metallicity in galaxies, and have also shown that hierarchical clustering scenarios may form galactic objects that resemble Milky Way-type galaxies from a chemical point of view. However, the SPH models with chemical implementations hitherto published are restricted to the Galaxy. It would be very important for the study of the formation and evolution of galaxies to be able to analyse a variety of galactic objects with different evolutionary histories. Hydrodynamical cosmological simulations are more suited to tackle this problem since the non-linear evolution of the matter is naturally accounted for, and, physical processes can be more consistently implemented. These models can provide coherent well-described environments for all objects and a complete record of their formation and evolution. The drawback is the treatment of numerical resolution effects.

In this paper, we concentrate on the description of the chemical model that has been implemented in a cosmolog-

ical hydrodynamical AP3M. First results on galaxy formation, global chemical properties and comparison with observations are reported. The detailed analysis of the chemical properties of the ISM and stellar population in galaxy-like objects such as abundance gradients, age-metallicity relations, etc., are given by Tissera et al. (2000, hereafter Paper II).

This paper is organized as follows. Section 2 describes the star formation process and the metal enrichment implementation. In Section 3 we assess the performance of the chemical model. In Section 4 we present the first results on galaxy formation and chemical evolution. Section 5 summarizes the results.

## 2 NUMERICAL MODEL

We use a cosmological numerical code based on the SPH technique described by Tissera et al. (1997). The SPH algorithm has been coupled to the AP3M gravitational code (Thomas and Couchman 1992), in order to follow the gravitational and hydrodynamical evolution of particles within a cosmological context. For the sake of simplicity, and as first step in the development of this chemical cosmological code, simulations have been run considering that the gas cools down by using the approximation given by Dalgarno and McCray (1972).

### 2.1 Star formation

In general, the modelling of star formation (SF) in SPH simulations is based on the Schmidt law and a series of hypothesis to select suitable SF regions. However, how it is actually implemented within each particular code depends on the different authors (e.g., Katz 1992; Navarro and White 1994; Tissera et al. 1997). In this paper, we describe a modified version of the SF implemented by Tissera et al. (1997) in order to be able to track the transformation of gas into stars in more detail, within a given gas particle.

We include the SF algorithm as follows. Gas particles are eligible to form stars if they are cold ( $T < T_*$ ) and satisfy a density criterium:  $\rho_{\text{gas}} > \rho_{\text{crit}}$ . This density criterium arises by requiring the cooling time of a gas particle to be smaller than its dynamical time. The critical temperature  $T_*$  is taken as the minimum provided value by the cooling functions ( $T_* \sim 10^4 \text{K}$ ). Finally, gas particles have to be part of a collapsing region. This requirement is imposed by selecting particles in a convergent flow ( $\nabla \cdot \vec{v} < 0$ ). When a gas particle satisfies all these conditions, star formation occurs according to the Schmidt law,

$$\frac{d\rho_{\text{star}}}{dt} = c \frac{\rho_{\text{gas}}}{t_*} \quad (1)$$

where  $c$  is the star formation efficiency and  $t_*$  is a characteristic time-scale assumed to be proportional to the dynamical time of the particle ( $t_* = t_{\text{dyn}} = (3\pi/16G\rho_{\text{gas}})^{1/2}$ ). Then, each stellar mass formed in a particle at a certain SF episode is given by  $\Delta\rho_{\text{star}} = C \rho_{\text{gas}}^{3/2} \Delta t$ , where  $\Delta t$  is the time step of integration ( $\Delta t = 1.3 \times 10^7 \text{ yr}$ ) and  $C$  a new SF efficiency. Note that, according to equation (1), in order to go from density to mass, the volume of the new-born stars has to be assumed. Taking into account that the process we are

modelling happens *within a gas particle* and, that according to observations, SF occurs normally in clusters, not in isolation, we assume that the volume occupied by the fraction of new-born stars is constant for all them. Thus, it can be absorbed in the new constant,  $C$ .

According to this SF scheme, in a given baryonic particle there could be several SF episodes that had occurred at different times. The gaseous mass of the baryonic particle is reduced by  $\Delta_{\text{star}}$  until its gas reservoir is depleted. A minimum gas mass equal to 5 % of the initial gas mass component is left over in each particle. When a particle reaches this minimum mass, it is transformed completely into a star particle and hereafter behaves as collisionless matter. Each  $\Delta_{\text{star}}$  formed can be followed up in time. The number of stars of a given mass within  $\Delta_{\text{star}}$  is estimated by assuming an Initial Mass Function (IMF). Hence, a baryonic particle may be formed by a gaseous and stellar components in different proportions according to its history of evolution (hereafter, hybrid particle). The stellar component can be made up of different stellar populations with different ages and chemical properties, which have been formed at different SF episodes. The chemical properties of each stellar population ( $\Delta_{\text{star}}$ ) reflect the chemical state of the ISM at the time of its formation.

The decoupling between gas and stars depends on the actual rate at which stars are formed in each baryonic particle, that, on its turn, depends on each evolutionary path. Hybrid particles may introduce some numerical artifacts since the stellar populations follow the gas evolution when they should probably not. However, this is not a trivial problem that can be easily resolved. An improvement of the decoupling process is under work and will be presented in a separate paper.

## 2.2 Metal Production

Metals are produced and ejected to the interstellar medium at the end of the life of stars. Most of chemical elements are ejected by Type II supernovae (SNeII) except for the iron that is mainly produced by Type I supernovae (SNeI). Particles are assumed to be initially formed by Hydrogen and Helium in primordial abundances ( $H = 0.75$ ,  $He = 0.25$ ). The first generations of stars with primordial abundances immediately enrich the ISM from where the new generations are born. It has to be stressed that we are not including the effects of (thermal or kinetic) energy injection into the ISM due to SN explosions. For the sake of simplicity we have splitted the treatment of the feedback problem into two stages. Firstly, we include chemical enrichment (this paper), and in a second step, we will intend to develop an energy feedback model. There have been several attempts to implement energy feedback in SPH codes by either injecting thermal (e.g., Katz 1992) or kinetic (e.g., Navarro & White 1994; Metzler & Evrard 1994; Navarro & Steinmetz 2000; Springel 2000) energies to the gas component due to SN explosions. However, these methods are still controversial leaving this problem as an open question for galaxy formation.

Let us now describe the nucleosynthesis prescriptions adopted in this model:

*Type II SNe:* We assume that stars more massive than  $8 M_{\odot}$  end their lives as Type II SNe. In order to estimate their number, we adopt a Salpeter IMF with a lower and up-

per mass cut-off of 0.1 and  $120 M_{\odot}$ , respectively. The IMF adopted gives the total number of SNeII formed in a certain range of stellar masses in a given  $\Delta_{\text{star}}$  at a certain time. Supernovae are thought to eject their whole metal production within a few  $10^7$  yr. In particular, we assume that their life-time is equal to the integration time-step of the simulations.

For comparison, we resort to both Portinari, Chiosi and Bressan (1998, P98) and Woosley and Weaver (1995, WW95) metal ejecta models and follow the evolution of different elements according to the information provided by the authors. P98 give metal yields for stars up to  $120 M_{\odot}$ , while WW95 assume that stars larger than  $40 M_{\odot}$  end up their lives as black holes. We consider the following elements according to each author: H, He<sup>4</sup>, C<sup>12</sup>, O<sup>16</sup>, Mg<sup>24</sup>, Si<sup>28</sup>, Fe<sup>56</sup>, for both P98 and WW95, and also, N<sup>14</sup>, Ne<sup>20</sup>, S<sup>32</sup>, Ca<sup>40</sup>, Zn<sup>62</sup>, for WW95.

*Type I SNe:* Following Matteucci and Francois (1989), we assume that supernovae Ia originate from carbon deflagration in C-O white dwarfs in binary systems. It is assumed that the masses of these binary systems are likely to be in the range 3 – 16  $M_{\odot}$ . The adopted nucleosynthesis prescriptions are taken from Thielemann, Nomoto and Hashimoto (1993). Type Ib SNe are assumed to be half the total number of Type I SNe and to produce only iron ( $\approx 0.3 M_{\odot}$  per explosion).

The main interest in including SNI events in the models is that they contribute with a substantial amount of iron. This element is fundamental to attempt to reproduce several observational results (see also Chiappini et al. 1997). The relative rate of SNI to SNII explosions has been observationally estimated in the solar neighbourhood and from extragalactic sources (van der Bergh 1991). These estimations suggest a range of possible values for the total SNI rate respect to that of SNII of  $2 \leq \text{SNRII}/\text{SNRI} \leq 3.11$ .

Binary systems evolve for a certain period of time ( $t_{\text{SNI}}$ ) during which mass is transferred from the secondary to the primary star until the Chandrasekhar mass is exceeded and an explosion is triggered. It is generally assumed that a fair fraction of SNeI will explode after a period of  $t_{\text{SNI}} \approx 10^8 - 10^9$  yr (Greggio 1996). It is straightforward to estimate when SNeI will explode and eject metals to the neighbouring region, since the formation time of each  $\Delta_{\text{star}}$ , in a given baryonic particle, is known. The effects of varying both the SNRII/SNRI relative rate (hereafter,  $\Theta_{\text{SN}}$ ) and  $t_{\text{SNI}}$  are analysed and results are confronted with observations in the following Sections.

To sum up, the free parameters of our chemical model are: star formation efficiency ( $C$ ), the initial mass function (IMF), its upper and lower mass cut-offs, the relative rate of different types of supernovae ( $\Theta_{\text{SN}}$ ), the life-time of binary systems that end as SNeI ( $t_{\text{SNI}}$ ) and the yields. Regarding the IMF, we are going to adopt a constant and unique one throughout this paper.

## 2.3 Model for metal ejection

How the chemical elements are distributed and mixed in the interstellar medium is a complex problem which is far from being solved from a theoretical point of view (e.g., Tenorio-Tagle et al. 1999). Furthermore, numerical simulations do not reach enough resolution to properly treat this small-scale

mixing process together with the process of galaxy assembly. Hence, the ejection and mixing of elements have to be modelled in heuristic way.

We use the SPH technique to distribute the metals within the neighbouring sphere of the  $j$  particle where a  $\Delta_{\text{star}}$  is formed. According to this technique, the value of a certain parameter at the location of  $j$  particle can be estimated by using the information stored in its neighbourhood, which is determined by its  $i$  neighbouring particles within its smoothing length ( $h_j$ ).

Using this concept, we can define the total mass ( $M_j^k$ ) of a given  $k$  chemical element ejected by a  $j$  particle due to SNeI or SNeII, as

$$M_j^k = \sum_{i=1}^{n_v} m_i / \rho_i M_j^k W(r_i - r_j, h_{ij}) \quad (2)$$

where  $n_v$  is the number of  $i$  neighbours of the  $j$  particle ( $n_v \approx 40$ ),  $m_i$  and  $\rho_i$  the gas mass and density of the  $i$  particle, respectively,  $W(r_i - r_j, h_{ij})$  and  $h_{ij}$ , the symmetrized kernel and smoothing length, respectively. In this scheme, each  $i$  neighbouring particle gets a contribution of each metal defined by

$$M_i^k = m_i / \rho_i M_j^k W(r_i - r_j, h_{ij}) \quad (3)$$

The  $j$  particle where the stellar mass has just formed is also included in this process. The masses of H and He are proportionally decreased according to the metal mass received by each particle, so that its total mass is always conserved.

The distribution of metals by using the SPH technique allows to spread out metals and enrich gas particles that may have not experienced SF but are close enough to other SF regions, working as an effective mixing mechanism. Note that gas particles can be enriched by more than one neighbour at each time-step. It has to be mentioned that numerical resolution would affect the mixing of metals since it also affects the determination of the neighbours. In Section 3, we will discuss this point in more detail. In the present implementation, metal mixing occurs only tied to the SF process, in the sense that, only new-born elements are distributed.

One of the advantage of this implementation is that particles move according to the equations of gravitation and hydrodynamics, leaving behind the closed-box hypothesis, among others. Particles with different astrophysical and chemical properties are mixed, particularly during violent events such as interaction and mergers, so that reproducing observations becomes a more challenging task.

### 3 TESTS

We carry out a series of simple tests to assess the effects of both, numerical resolution and the variation of the different parameters ( $C$ ,  $\Theta_{\text{SN}}$ ,  $t_{\text{SNI}}$ ) on the chemical properties of baryons. We also intend to evaluate the dependence of the results on the two adopted nucleosynthesis models, P98 and WW95. For this purpose, we follow the evolution of a homogeneous gaseous sphere. The sphere is represented by  $10^3$  gas particles initially distributed following a density profile  $\rho \propto r^{-2}$ , in a radius of 625 kpc, without a dark matter halo. This simple experiment gives a clear idea of how each pa-

rameter affects the chemical properties of baryons and have the advantage of a low computational cost.

#### 3.1 Effects of numerical resolution

Numerical problems may affect both, the process of star formation and specially the distribution of metals. With respect to the former, if dark matter haloes in galactic objects are numerically well resolved, the star formation process may not be strongly affected by the numerical resolution (see discussion in Domínguez-Tenreiro, Tissera and Sáiz 1998). This is due to the fact that dark matter determines the potential well on to which the gas settles on. If dark matter haloes are well resolved, baryons are forced to distribute adequately. In this way, the gas density profiles are well reproduced and the SF can be correctly followed (Tissera 2000). Nevertheless, the gas component has to be resolved, at least, by few hundred particles (Navarro and White 1994). In our simulations, baryonic and dark matter components are represented by particles of equal mass. Therefore, dark matter haloes are resolved by a much larger number of particles than the baryonic component. Hence, the potential wells of the larger galactic haloes are very well defined (see Tissera and Domínguez-Tenreiro 1998). Consequently, we restrict our global analysis to galactic objects resolved with more than 250 baryonic particles.

On the other hand, the radius of the neighbouring sphere in which the metals produced by the stellar component are distributed is affected by the numerical resolution of the experiment. Consequently, this problem may have a non-negligible effect on the metal distribution and the chemical properties of gas and stars, and requires a more detailed analysis. For this purpose, we have studied the evolution of two gaseous spheres without dark matter haloes. Each of them represents a system with total gaseous mass of  $1.3 \times 10^{11} M_{\odot}$  and initial radius of 615 kpc. One of the experiments (E1) resolves the sphere with  $10^3$  particles ( $m_p = 1.3 \times 10^8 M_{\odot}$ ), while the second experiment (E1H) has higher numerical resolution:  $8 \times 10^3$  gas particles ( $m_p = 1.7 \times 10^7 M_{\odot}$ ). Since these spheres have no dark matter haloes, taking into account the former discussion, it is reasonable to expect that their star formation histories will be different. In fact, the sphere in E1H starts forming stars before its counterpart in E1. However, the effects that this earlier SF has on their metallicity is not dramatic, as it can be observed from Fig.1, where we have plotted the mean values of [O/Fe] vs. [Fe/H] for both experiments. The greatest differences are obtained for the low metallicity stars ([Fe/H]  $< -3$ ) due to the fact that star formation begins before in E1H and has a greater intensity than SF in E1. As stars with higher metallicities are formed, this difference diminishes. Note that error bars in E1H comprise the distribution of E1 for [Fe/H]  $> -4$  (except for the first point).

The main difference observed between these two experiments is that low numerical resolution produces a reduction in the dispersion of the distribution as can be seen from the error bars in Fig.1. This fact can be understood by considering that, in the experiment with lower resolution, the neighbouring sphere ( $n_v \sim 40$ ) comprises a larger volume, thus producing a more effective mixing of the metals in the gas. Conversely, when numerical resolution is increased, the new elements produced by a certain particle are distributed

in a smaller volume. This leads to a less efficient mix at the scale of the system, producing an increase in the metallicity dispersion. We cannot theoretically assess at what extent this dispersion has any physical meaning since the mixing mechanisms in galaxies are not yet well understood. It might be possible that SN explosions spread metals in larger volumes than that provided by the SPH technique. This fact would produce a more uniform-metal distributions in the interstellar medium, as it actually occurs in the low numerical resolution run.

Taking into account these experiments, we conclude that the main effect of using the SPH technique to distribute metals is that the better resolved objects (i.e., those with higher number of baryonic particles that, in our simulations, implies larger masses) would have a larger dispersion in their chemical properties than the smaller ones. Mean values of the quantities will be considered as adequate estimations.

### 3.2 Effects of the variation of the star formation parameters

We are now going to analyse the effects that the different chemical model parameters have on the properties of the stellar populations of the spheres.

As can be seen from Table 1, experiments E1, E2 and E3 differ among each other in the life-time of binary systems that end up as SNeI. The values considered are  $10^8$ ,  $4 \times 10^8$  and  $10^9$  yr, respectively. The SF efficiency and  $\Theta_{\text{SN}}$  used are the same in these three experiments. The ratio  $[\text{O}/\text{Fe}]$  vs.  $[\text{Fe}/\text{H}]$  clearly illustrates the effects of varying the parameters. Fig.2 shows  $[\text{O}/\text{Fe}]$  vs.  $[\text{Fe}/\text{H}]$  for these three experiments at different stages of evolution. As can be seen from this figure, as soon as the first stars are formed, the differences among them are very important. The smaller  $t_{\text{SNI}}$  used in E1 allows a rapid production of Fe and, consequently, the number of low metallicity stars ( $[\text{Fe}/\text{H}] < -3$ ) is considerably lower than in E2 and E3, for all times. The larger  $t_{\text{SNI}}$  value adopted in E3 produces a dex difference in the ratio  $[\text{O}/\text{Fe}]$  compared to the values in E1 and E2 for  $t = 1.13 \times 10^{10}$  yr. As time goes on, all experiments reach solar values, although, the variation of  $t_{\text{SNI}}$  among them leads to appreciably different evolutionary paths. For E1 and E2, the  $[\text{O}/\text{Fe}]$  is above observed values for the solar neighbourhood, and the steepness of the relation is much abrupt for  $[\text{Fe}/\text{H}] > -1$ . Experiment E1 ( $t_{\text{SNI}} = 10^8$  yr) gives a more consistent relation for stars with  $[\text{O}/\text{Fe}] < 1$ . In this case, the final shape and range of abundances values are set as soon as the first stars formed which implies that even at early stages of evolution, this combination of SN parameters can produce stellar populations with metal contents up to solar.

In Fig.3, we show the same relations for experiments E4, E5 and E6. In E4 we have changed the relative ratio  $\Theta_{\text{SN}}$  from 2 (in E1) to 4. Since SNRII is the fraction of stars with masses greater than  $8 M_{\odot}$  in a certain time-step, given by the IMF adopted, an increase in the ratio  $\Theta_{\text{SN}}$  implies a decrease of SNRI. The effect of the variation of this parameter gives the expected differences in the abundance tracks. Note that there is no change in the slope of the  $[\text{O}/\text{Fe}]$  vs.  $[\text{Fe}/\text{H}]$  relation, but the abundances in E4 do not get to solar values because there are not enough SNeI to produce the necessary amount of Fe.

In experiment E5 we use a higher SF efficiency than

that in E1. In this case, stars are formed faster and the gas is enriched very efficiently so that the new-born stars immediately evolve to higher metallicity regions. As a consequence, the low-metallicity tail in the  $[\text{O}/\text{Fe}]$  vs.  $[\text{Fe}/\text{H}]$  relation vanishes. Note that the higher the  $C$  value used, the larger the stellar masses ( $\Delta_{\text{star}}$ ) formed, so that the number of SF events in a given baryonic particle diminishes. This is the reason why the number of points in E5 is smaller when compared to the distribution in E1. The important aspect to remark is that, in E5, the range of metallicity covered by the stellar populations is considerably smaller. This implies that a very efficient SF process can enrich the medium to solar values very quickly so that most of stars would tend to be located in the high metallicity region.

The comparison between experiments E1 and E6 clearly illustrates how the simulation results depend on the two yield models, P98 and WW95. The features of the  $[\text{O}/\text{Fe}]$  vs.  $[\text{Fe}/\text{H}]$  relation in E6 can be appreciated in the bottom row of Fig.3. The main characteristic observed for this experiment, where P98 yields were used, is the lack of the low-metallicity tail ( $[\text{Fe}/\text{H}] < -3$ ), which can be appreciated in E1. On the other hand, the low-metallicity stars in E6 ( $[\text{Fe}/\text{H}] < -2$ ), have almost constant values of  $[\text{O}/\text{Fe}]$ , in contrast with the results of E1, where a gradient is observed. This difference arises because P98 yields produce more iron with respect to the other elements than WW95, up to an order of magnitude more, in some cases. So, stars are rapidly brought to lower abundances ratios with respect to iron. Despite this fact, these relations are quite similar, with exception that WW95 seems to reach slightly higher metallicities values for the same model parameters at  $z = 0$ . This fact implies that P98 yields for enriched stars produce, in general, more elements than those of WW95. The comparison of other chemical elements shows that the major difference is in the  $[\text{C}/\text{Fe}]$  vs.  $[\text{Fe}/\text{H}]$  relation. In Fig.4, we show this relation for experiments E1 and E6 as a function of time. As clearly seen in the case of E6, there is an excess of carbon in relation to iron for  $[\text{Fe}/\text{H}] > -1.2$  that produces a positive gradient.

To sum up, we find that all SF and SN parameters have non-negligible effects on the chemical properties of baryons. Then, in order to choose the correct combination of SN and SF parameters, a detailed comparison with observations has to be done.

## 4 GALAXY FORMATION

We are now interested in applying this model to the study of galaxy formation in a cosmological framework. As a first step, we look at the global properties of galaxy-like objects (GLOs) and compare them with observations. The different formation and evolutionary histories of each GLO (i.e., collapse time, merger tree, properties of progenitors, interactions, etc.) may affect their SF and chemical content in a complex way so that, even in the same experiments, GLOs may exhibit different characteristics. This fact makes of cosmological simulations a very useful tool for chemical evolution studies.

The traditional model to study chemical evolution is the so-called One-Zone Simple Model based on two main assumptions: the system is isolated (i.e, no inflows or out-

**Table 1.** Test: Main Parameter

S	$C$	$\Theta_{\text{SN}}$	$t_{\text{SNI}}$	yields
E1	5e-6	2	1	WW95
E2	5e-6	2	4	WW95
E3	5e-6	2	10	WW95
E4	5e-6	4	1	WW95
E5	5e-2	2	1	WW95
E6	5e-6	2	1	P98

Units:  $[t_{\text{SNI}}] = 10^8 \text{ yr}$  ;  $[C] = Mpc^{9/2}/M_{\odot}^{1/2}/yr$ .

flows) and well-mixed (i.e., instantaneous recycling), at all times (van der Bergh 1962; Schmidt 1963; Tinsley 1980). Other hypothesis are related to the initial condition of the gas, IMF and nucleosynthesis yields. We remark the first two assumptions since they are inconsistent with the formation and evolution of galaxies in a hierarchical clustering scenario. In our experiments, structures form within a cosmological model suffering physical processes such as mergers, encounters, inflows, etc., which may affect the dynamics and kinematics of the dark and baryonic matters. Although some authors have included inflows and relaxed the hypothesis of instantaneous recycling (e.g., Chiappini et al. 1997), these models are not formulated in a cosmological framework and do not include dynamical effects that may affect the SF process and the mixing of chemical elements. Regarding the IMF and initial condition of the gas, we adopt a Salpeter IMF for all times, and the gas is assumed to be initially in primordial abundances.

#### 4.1 Numerical Experiments

We performed SPH simulations consistent with a Cold Dark Matter (CDM) spectrum with  $\Omega = 1$ ,  $\Lambda = 0$ ,  $\Omega_b = 0.1$ , and  $\sigma_8 = 0.67$ . We used  $N = 262144$  particles ( $M_{\text{part}} = 2.6 \times 10^8 M_{\odot}$ ) in a comoving box of length  $L = 5h^{-1} \text{ Mpc}$  ( $H_0 = 100h^{-1} \text{ km s}^{-1} \text{ Mpc}^{-1}$ ,  $h = 0.5$ ), starting at  $z = 11$ . Note that dark matter and baryonic particles have the same mass. The gravitational softening used in these simulations is 3 kpc, and the smaller smoothing length allowed is 1.5 kpc. Simulations S1 to S5 share the same initial conditions while S6 shares the SF and SN model parameters of S2, but has different random phases.

Simulations include SF and metallicity effects as described in Section 2. According to the discussion carried out in the previous Section, the value of  $C$ ,  $\Theta_{\text{SN}}$  and  $t_{\text{SNI}}$  affect the chemical composition of the stellar and gaseous components. In order to assess the impact of these parameters on the chemical properties of galactic objects, we have performed simulations with the same initial condition but varying the model parameters (see Table 2). We also compare results from simulations where the two adopted yields, P98 and WW95, have been used. We will focus on the study of global chemical properties of the ISM and the stellar populations of GLOs, and their relation with the dynamical parameters of the objects.

In order to study the properties of GLOs at  $z = 0$ , we identify them at their virial radius ( $\delta\rho/\rho \approx 200$ ; White and Frenk 1991). In Table 3 we give their total dark matter ( $N_{\text{dark}}$ ) and baryonic ( $N_{\text{bar}}$ ) number particles within the virial radius and their virial circular velocity ( $V_{\text{vir}}$ ). Letter b in the label code of the GLO (second column, Table 3)

indicates if the main baryonic system is formed by a pair of galactic objects. From the set of GLOs identified, we are only going to analyse those with more than 250 baryonic particles within their virial radius.

As it is well known, GLOs are formed by a dark matter halo that generally hosts a main baryonic clump and a series of satellites. All quantities measured at the virial radius are related to these complex systems. However, if we want to confront the simulated results with observations, it has to be taken into account that observed astrophysical quantities come from the luminous matter. For this purpose, we define a galactic object (GAL) as the structure determined by the main baryonic clump (including the dark matter mixed within it) hosted by a GLO.

The radius that encloses 83% of the luminous mass of an exponential disc corresponds to the isophote of 25 mag  $\text{arcsec}^{-2}$ . Assuming a mass-to-luminosity ratio equal to 1, we define the optical radius of a GAL as the one that encloses 83% of its baryonic mass. All chemical and astrophysical properties will be referred to two optical radius ( $2R_{\text{opt}}$ ), unless otherwise stated (see Table 3). This definition allows us to carry out a more meaningful comparison with observations. In this respect,  $V_{\text{opt}}$ , defined as the circular velocity at  $2R_{\text{opt}}$ , is determined by the baryonic and dark matter distributions in GALs, and consequently, it is related to the physical mechanisms responsible for the concentration and distribution of the matter in the central region of a GLO (i.e., star formation, mergers, gas inflows, environment). Conversely,  $V_{\text{vir}}$  is a global parameter determined by the total potential well of the system.

Recall that, in these simulations, there are three types of baryonic particles: pure gaseous, hybrid and total stellar ones. We identify those that belong to a given GLO and its GAL, and look at their chemical properties within  $2R_{\text{opt}}$  at  $z = 0$ .

#### 4.2 Global Chemical Properties

In this Section we study the correlations between chemical and dynamical properties of the GALs, in order to explore the possible physical mechanisms that may determine the metallicity of a galaxy, and to assess the dependence on model parameters.

Observationally, defining the metallicity of a galaxy is a complex matter since it depends on the type and quality of available data, the element used as the estimator, etc. (e.g., Kunth and Ostlin 1999). Moreover, observations only give information on the metallicity of certain regions within a galaxy so that they could be considered good estimators of the global metallicity only if the ISM were efficiently mixed.

Let us first review the main hypotheses of the one-zone

**Table 2.** Cosmological Simulations

S	C	$\Theta_{\text{SN}}$	$t_{\text{SNI}}$	yields
S1	5e-6	2	1	P98
S2	5e-6	2	1	WW95
S3	5e-4	2	1	WW95
S4	5e-4	3	5	WW95
S5	5e-5	2	1	WW95
S6	5e-6	2	1	WW95
S7	5e-6	2	1	WW95

Units:  $[t_{\text{SNI}}] = 10^8$  yr;

$$[C] = \text{Mpc}^{9/2} / \text{M}_{\odot}^{1/2} / \text{yr}.$$

Simple Model in order to understand the differences and advantages of our chemical scheme. The two basic assumptions of the Simple Model are: a) the system is isolated and b) it is well mixed at all times. It is also generally assumed instantaneous recycling.

Concerning hypothesis a), our galactic objects form in consistency with a hierarchical clustering scenario via the aggregation of substructure. At  $z = 0$  a galactic object generally consists of a dark matter halo, a main baryonic clump and a series of satellites. Even if the objects do not have nearby similar-mass objects, they are rarely isolated. Moreover, there are always both, gas infall from the dark matter haloes and encounters with satellites that may tidally induce gas inflows as have been reported in numerical (e.g., Mihos & Hernquist 1996; Tissera 2000) and observational works (Barton, Geller & Kenyon 1999). At higher  $z$ , interactions and mergers notably increase so that the hypothesis of 'closed-box' is never valid since what is observationally identified as a galaxy is just a component of the whole system. It has also to be stressed that the star formation history is affected by the evolution of the galactic object. This evolutionary process determines the different chemical properties of the objects in our simulations (see Tissera et al. 2000 for details).

Due to the mixing mechanism adopted which depends on the local gas density, and the fact that the systems are never isolated, the metallicity of the gas and the new-born stellar population is not uniform. At a given time, we found a significant spread in the values of the ISM metallicities within a given GAL (Tissera et al. 2000). These results are consistent with those from chemodynamical models (e.g., Samland et al. 1997). Regarding instantaneous recycling, we follow the evolution of the populations according to the stellar masses including supernovae I and II explosions. A consistent implementation of SNeI is performed as described in Section 2.2. Planetary nebulae (PNe) have not been included in this work.

Unfortunately we cannot treat in as much detail the ISM as chemodynamical models do, but this drawback is compensated by the fact that galaxy formation is well-described according to a cosmological framework without ad-hoc hypotheses. Moreover, the coupled non-linear evolution of dark matter and baryons has non-negligible effects on the star formation (e.g., Navarro & Steinmetz 2000; Tissera et al. 2000) that is directly related to the enrichment process.

We will first attempt to assess which dynamical parameters correlate with the chemical properties of the GALs. We define global quantities for the chemical content of GALs. A global metallicity ( $Z$ ) is assigned to the stellar popula-

tion and to the gaseous component of a GAL, taking into account all contributions from either, the stars or the gas respectively, according to

$$Z_a = \frac{\sum_{k=1}^n M_k}{M_a} \quad (4)$$

where  $a$  refers to the component (i.e., stars or gas),  $M_k$  is the total mass of the  $k$  chemical element present in the  $a$  component,  $n$  is the total number of  $k$  chemical elements considered, and  $M_a$  is the total mass of the  $a$  component within two optical radius. The estimated  $Z_{\text{star}}$  and  $Z_{\text{gas}}$  for each GAL are listed on Table 3.

We have analysed the GALs formed in simulations S2, S6 and S7. These experiments have the same star formation and cosmological model parameters but different random phases in the initial conditions. The SN parameters used in these experiments are taken from the best results given by the test runs ( $t_{\text{SNI}} = 10^8$  yr,  $\Theta_{\text{SN}} = 2$ ). In Fig.5a and Fig.5c we show the global metallicities of the stellar population ( $Z_{\text{star}}$ ) and the gaseous component ( $Z_{\text{gas}}$ ) of the GALs versus their gas fractions. We find the expected trend indicating that the smaller the left-over gas, the higher the metallicity. Note that the slope of this relation for the gas and the stars is different, being steeper for the former. The averaged values of global metallicities for these runs are:  $\langle Z_{\text{star}}/Z_{\odot} \rangle = 0.25 \pm 0.05$  and  $\langle Z_{\text{gas}}/Z_{\odot} \rangle = 0.24 \pm 0.09$ . Note that we are considering the metal content of stars and gas particles within  $2R_{\text{opt}}$  irrespectively of their particular location. These mean metallicity values cannot be directly compared to that of disk stars in the solar neighbourhood.

In Fig.5b and 5d, we plot  $Z_{\text{star}}$  and  $Z_{\text{gas}}$  versus the total stellar mass ( $M_{\text{star}}$ ) within  $2R_{\text{opt}}$ . As can be seen there is no clear trend between these parameters, albeit a weak tendency to have the higher metallicities in both, gaseous and stellar components of GALs with intermediate stellar masses:  $3 \times 10^{10} M_{\odot}$  to  $6 \times 10^{10} M_{\odot}$ .

For comparison, we have estimated these relations for our GALs assuming they have behaved according to the Simple Model. We include three cases:  $0.2Z_{\odot}$  (dotted-dashed lines),  $0.5Z_{\odot}$  (solid lines) and  $Z_{\odot}$  (dashed lines). It can be appreciated the significant differences between the Simple Model and the results of the numerical simulations. The slope of  $Z_{\text{star}}/Z_{\odot}$  versus  $M_{\text{gas}}/M_{\text{bar}}$  is different as well as the systematic increase of stellar metallicity as a function of the stellar mass formed in the Simple Model which contrasts with the behaviour of the numerical simulations. By inspection of the same relation for the gaseous components, we find that the Simple Model overestimates the metallicity of the galactic gaseous components for the parameters that match the chemical distribution of the stars. Hence,

**Table 3.** Galaxy-like Objects: Main Parameters

S	GLO	$N_{\text{dark}}$	$N_{\text{bar}}$	$V_{\text{vir}}$	$R_{\text{opt}}$	$V_{\text{opt}}$	$M_{\text{star}}$	$Z_{\text{gas}}/Z_{\odot}$	$Z_{\text{star}}/Z_{\odot}$
S1	596	4049	542	137.67	23.68	224.67	5.45	0.45	0.46
	538	4574	576	143.04	16.46	203.47	1.83	0.28	0.45
	538b	4655	588	143.92	19.16	186.41	3.46	0.49	0.45
	536	5036	636	147.74	19.89	243.13	6.25	0.48	0.47
	456	6297	931	160.18	18.09	261.21	8.07	0.54	0.39
	426	2433	343	116.41	12.36	200.53	2.60	0.45	0.44
	421	1848	267	106.11	19.61	166.06	1.43	0.26	0.31
	334	1848	267	106.31	19.61	166.05	1.43	0.26	0.31
	347	5752	724	154.41	14.06	246.20	5.46	0.61	0.45
	347b	5727	726	154.20	12.22	196.96	2.56	0.49	0.51
	325	5385	699	151.23	8.28	280.88	5.25	0.49	0.36
	312	1858	271	106.54	14.08	190.47	2.12	0.46	0.46
	221	1991	285	108.93	7.63	208.03	3.14	0.56	0.47
S2	596	4034	541	137.45	18.99	301.70	5.85	0.19	0.34
	538	4591	584	143.29	18.74	251.69	2.37	0.17	0.24
	538b	4637	589	143.77	11.25	246.80	3.24	0.21	0.27
	536	5019	627	147.46	14.82	319.25	6.57	0.20	0.30
	456	6322	932	160.35	21.63	323.83	7.36	0.19	0.23
	426	1828	315	106.79	5.60	290.85	4.60	0.37	0.36
	421	2466	340	116.83	12.50	256.97	2.18	0.17	0.19
	334	1863	266	106.48	23.28	203.43	1.67	0.09	0.24
	347	5770	720	154.52	14.64	308.19	5.41	0.27	0.29
	347b	5715	721	154.10	9.19	249.24	2.73	0.22	0.28
	325	5478	703	152.01	12.91	315.70	5.37	0.23	0.21
	312	1840	271	106.24	15.67	239.76	2.23	0.19	0.21
	221	1978	289	108.78	29.99	217.00	2.98	0.23	0.23
S3	596	4061	545	137.80	18.12	306.16	6.37	0.39	0.52
	538	4570	590	143.16	9.67	258.72	3.42	0.59	0.64
	538b	4541	588	142.85	22.15	246.53	2.68	0.20	0.34
	536	5004	629	147.40	17.18	327.41	7.18	0.20	0.27
	456	6536	935	161.95	15.33	332.28	10.78	0.25	0.65
	426	2451	339	116.56	7.26	263.70	2.61	0.48	0.47
	421	1703	320	104.72	4.26	286.90	5.47	0.38	0.53
	334	1847	273	106.00	18.54	210.09	2.23	0.17	0.60
	347	5874	724	155.37	38.15	337.76	9.57	0.16	0.29
	325	5502	714	152.32	9.28	327.38	5.98	0.26	0.33
	312	1876	275	106.89	13.97	239.87	2.63	0.17	0.26
	221	2009	293	109.32	7.18	249.48	2.55	0.21	0.37
S4	596	4061	545	137.80	18.12	306.16	6.37	0.17	0.25
	538	4570	590	143.16	9.67	258.72	3.42	0.18	0.25
	538b	4541	588	142.85	22.15	246.53	2.68	0.13	0.25
	536	5004	629	147.40	17.18	327.41	7.18	0.18	0.21
	456	6536	935	161.95	15.33	332.28	10.78	0.21	0.32
	426	2451	339	116.56	7.26	263.70	2.61	0.16	0.19
	421	1703	320	104.72	4.26	286.90	5.47	0.33	0.26
	334	1847	273	106.00	18.54	210.09	2.23	0.10	0.34
	347	5874	724	155.37	38.15	337.76	9.57	0.14	0.25
	325	5502	714	152.32	9.28	327.38	5.98	0.22	0.17
	312	1876	275	106.89	13.97	239.87	2.63	0.14	0.22
S5	596	4036	538	137.51	22.34	297.28	6.49	0.19	0.37
	538	4629	591	143.66	17.70	241.27	3.45	0.23	0.43
	538b	4520	577	142.55	720.66	247.62	2.43	0.14	0.26
	536	5037	640	147.75	14.53	328.11	7.38	0.24	0.33
	456	6326	933	160.41	17.73	327.90	9.25	0.25	0.29
	426	2446	344	116.59	11.46	259.62	2.85	0.24	0.25
	421	1842	271	106.29	22.11	206.27	1.95	0.11	0.28
	334	1842	271	106.29	22.11	206.27	1.95	0.11	0.28
	347	5771	723	154.48	13.65	309.75	6.35	0.30	0.37
	347b	5722	727	154.20	9.71	252.06	2.71	0.21	0.27
	325	5421	702	151.54	8.61	334.18	6.43	0.27	0.26



Table 3 – continued

S	GLO	$N_{\text{dark}}$	$N_{\text{bar}}$	$V_{\text{vir}}$	$R_{\text{opt}}$	$V_{\text{opt}}$	$M_{\text{star}}$	$Z_{\text{gas}}/Z_{\odot}$	$Z_{\text{star}}/Z_{\odot}$
S6	665	4552	626	143.30	7.54	287.46	3.44	0.20	0.21
	565	4408	626	141.97	4.03	151.72	0.64	0.15	0.23
	546	6452	895	161.04	6.14	357.70	6.86	0.22	0.19
	354	7421	961	168.28	4.28	349.50	5.71	0.19	0.20
	354b	2703	398	120.59	15.06	236.34	3.16	0.27	0.26
	235	3542	529	132.27	11.10	310.54	6.03	0.34	0.27
	234	1994	275	108.84	17.48	212.84	1.94	0.16	0.21
	235b	4213	612	139.89	20.71	279.96	5.41	0.23	0.32
	127	6892	797	163.51	21.66	329.06	7.08	0.21	0.28
	554	2748	385	121.21	8.98	268.50	3.60	0.28	0.27
S7	412	2583	340	118.32	5.26	231.50	2.00	0.22	0.29
	411	2214	338	113.20	3.81	145.39	0.92	0.25	0.31
	412b	4954	640	147.00	10.93	314.43	5.44	0.37	0.25
	344	2673	317	119.35	5.93	282.17	4.44	0.49	0.34
	261	2839	362	122.09	7.49	287.67	4.79	0.39	0.27
	215	3951	518	136.39	11.32	260.92	3.10	0.27	0.21
	215b	3884	510	135.67	18.21	223.06	1.57	0.16	0.19
	275	10743	1417	190.48	14.20	382.86	13.14	0.27	0.28
	232	8844	1204	178.73	5.95	403.29	7.78	0.16	0.18
	235	2162	244	110.95	3.50	195.64	1.93	0.42	0.25
	233	4002	574	137.52	10.37	257.12	3.73	0.30	0.31
	245	2206	258	111.88	8.03	250.97	2.97	0.30	0.30
	222	3148	412	126.46	8.00	286.05	5.11	0.36	0.30
	225	2474	370	117.37	13.47	258.48	3.98	0.26	0.22
	131	2292	244	112.97	18.75	191.21	0.57	0.09	0.11
	131b	2335	244	113.59	31.22	220.19	1.52	0.17	0.21
	134	6934	981	165.10	11.23	365.57	8.53	0.22	0.25
	135	9700	1311	184.27	10.60	364.38	6.89	0.17	0.19

$$[M_{\text{star}}] = 10^{10} M_{\odot}, [R_{\text{opt}}] = \text{kpc}.$$

$$[V] = \text{km s}^{-1};$$

it seems that it is not possible to reproduce simultaneously the trends found in the stellar population and the gas of the simulated GALs with the Simple Model. This is somewhat expected since our code takes into account more complex processes (such as mergers, interactions, gas infall, etc) that are not considered in the Simple Model.

We have studied the dependence of  $Z_{\text{star}}$  on  $V_{\text{vir}}$  and  $V_{\text{opt}}$  finding no significant correlations. We expected the lack of correlation with  $V_{\text{vir}}$  since it is determined by the whole gravitational bound system, while the chemical properties of the GALs are more strongly related to the fate of the baryonic matter in the internal regions. In fact, Fig.6a shows no significant trend between the stellar mass of the GALs and their virial velocity. On the contrary, there is a clear correlation of  $M_{\text{star}}$  with  $V_{\text{opt}}$  as can be seen from Fig.6b. If a universal value for the stellar mass-to-light ratio is assumed, this correlation would imply a Tully-Fisher relation similar to those found in previous works (e.g., Tissera et al. 1997; Navarro & Steinmetz 2000). Given that our GALs follow the Tully-Fisher relation, one would expect, in principle, a correlation of the stellar population metallicity with the  $V_{\text{opt}}$  which is not found. We think that this lack of correlation is due to the fact that the chemical properties of these GALs are also affected by their merger history. Violent events have a strong impact on the baryon distributions and, consequently, on the metals mixing (White 1981; Cora et al. 2000). Furthermore, these objects are continuously accreting gas that contributes with pristine material to form new stars. From these results we find that the mean metallicity of the stellar population of the GALs cannot be directly linked to the optical mass either. Note the lack of SN wind effects

in our simulations, as first discussed by Dekel & Silk (1986), could strongly affect the evolution of the gaseous component of low virial mass haloes, producing a non-negligible effect on the chemical properties of these systems.

We have also studied how the properties discussed above change for different nucleosynthesis yield models. We have analysed the relations shown in Fig.5 for experiment S1 which has been run with the same SF and SN parameters than those used in S2, but with the nucleosynthesis model of P98 instead of those of WW95. It can be seen in Fig.7a, a similar correlation than that shown in Fig.5a although with a shallower slope; and a lack of correlation between  $Z_{\text{star}}$  and  $M_{\text{star}}$  in Fig.7b. It can also be appreciated that global metallicities in the simulation with P98 model are higher than those in simulations using WW95 yields, with average values of  $\langle Z_{\text{gas}}/Z_{\odot} \rangle = 0.40 \pm 0.11$  and  $\langle Z_{\text{star}}/Z_{\odot} \rangle = 0.45 \pm 0.06$ . Hence, the different yields used imply significantly different results.

In order to explore the effects of changing the model parameters,  $\Theta_{\text{SN}}$ ,  $t_{\text{SNI}}$  and  $C$ , we plot in Fig.8  $Z_{\text{star}}$  versus  $M_{\text{gas}}/M_{\text{bar}}$  and  $M_{\text{star}}$  for simulations S3, S4 and S5 (see Table 2). By inspection to Fig.8a we can see that this correlation is present for all these experiments except S3. This simulation has the most efficient star formation, the largest value of  $C$ , which is an important parameter that strongly affect star formation and metallicity: for higher  $C$  values, and keeping the SN parameters fixed, the dispersion in metallicity increases. Note however that if the rate of SNeI is decreased (larger  $\Theta_{\text{SN}}$ ) and the  $t_{\text{SNI}}$  increased, this correlation is recovered (S4). Hence, these three parameters are relevant at determining the global chemical properties of the

GALs. In the case of the relation between metallicity and luminosity (total stellar mass), the correlation is not present as it can be seen from Fig.8b. However, we cannot further study the relative importance of the model parameters unless we look into more detail to the chemical properties of the gaseous and stellar components (to be analysed in Tissera et al. 2000).

Estimates of the mean  $Z_{\text{star}}$  and  $Z_{\text{gas}}$  values of GALs in each simulation (see Table 4) show that when the gaseous component is more gradually transformed into stars (S1, S2, S6, S7), the mean global metallicity of stellar populations and the ISMs at  $z = 0$  are very similar, independent of the nucleosynthesis yield models used. Conversely, when the SF efficiency is increased (S3, S4, S5), the difference between the mean  $Z_{\text{star}}$  and  $Z_{\text{gas}}$  becomes very important. In this case, most of the metals are locked into stars, regardless of the SN parameters. Hence, in our chemical model a very efficient SF process produces, on average, ISMs considerably less metal-rich than the stellar populations of the GALs.

However, it has to be noted that the mixing mechanism plays a key role in determining this result. A different implementation could lead to a more efficient distribution of metals in a shorter time-scale, quickly enriching the ISMs. Nevertheless, the way chemical elements are mixed in the ISM is still a controversial question that remains to be resolved from a theoretical and observational point of view.

Unfortunately, we cannot directly compare these results with those derived from analytical or chemodynamical model since the latter focus to the study of the Galaxy and do not have a sample where dependences with the dynamical parameters of the galactic objects could be studied. Raiteri et al. (1996), although describing a similar chemical model as the one studied in this paper and using the SPH technique, do not consider different galactic haloes so that we cannot compare our findings with their results.

### 4.3 Comparison with Observations

Observations of galactic and extragalactic HII regions and OB associations provide information about the chemical properties of the forming stellar population and the ISM. These observations give relations for some primary elements such as S, Ne, and C, and for the so-called secondary ones, like nitrogen, as a function of the ratio O/H. In this Section, we resort to these observational results to assess the global chemical properties of the stellar populations and ISM of the simulated GALs.

Concerning primary elements, Galactic and extragalactic HII regions show that the ratios (S/O) and (Ne/O) do not depend on (O/H). However, the dispersion in these ratios is quite large (Pagel 1997). The Simple Model actually predicts a similar behavior since in this scheme, the ratios between primary elements are constant. However, this model fails to reproduce the observed correlation between (C/O) vs. (O/H). A similar problem is detected for the observed (N/O) vs. (O/H) that exhibits a steeper correlation than that predicted by this model. Note that most observations are obtained from HII regions which are assumed good tracers of the metallicity of the galactic ISM.

We analyse the ISMs in our GALs, which are determined by the gas particle properties within  $2R_{\text{opt}}$ . The

global metallicity,  $Z_{\text{gas}}^k$ , for each  $k$  chemical element in the ISM of a GAL is defined as follows,

$$Z_{\text{gas}}^k = \frac{\sum_{i=1}^{n_p} m_i^k}{M_{\text{gas}}} \quad (5)$$

where  $n_p$  is the total number of  $i$  gas particles within  $2R_{\text{opt}}$ ,  $m_i^k$  is the mass of the  $k^{\text{th}}$  element in the  $i^{\text{th}}$  particle and  $M_{\text{gas}}$  is the total gas mass within  $2R_{\text{opt}}$ . An equivalent relation can be defined for the stellar population,  $Z_{\text{star}}^k$ .

In Fig.10, we plot  $\log(\text{S/O})$  for the ISM in the GALs in simulations S2, S3, S4 and S5. As it can be seen from this figure, the mean values obtained in the simulations are in very good agreement with observations (taken from Pagel 1997). The average  $\log(\text{S/O})$  for GALs shows a large dispersion that compares well with the observed values. The larger S/O ratios are obtained for the simulation with the highest SF efficiency (simulation S3). However, by changing SN parameters in order to diminish the effects of SNI explosions, and maintaining the same SF parameter in the simulation (simulation S4), we obtain substantially smaller abundance ratios and dispersions.

In Fig.11, we plot  $\log(\text{C/O})$  versus  $\log(\text{O/H})$  for GALs in simulations S2, S3, S4 and S5 (WW95) and simulation S1 (P98). We include observations of HII regions (Pagel 1997). A remarkable fact that can be seen from this figure is the large difference between the results of WW95 and P98 models. GALs in S1, which are exactly equivalent to those in S2, except for the nucleosynthesis model adopted, have ratios almost half an order of magnitude larger than their WW95 counterparts, and are out of the observational range. Conversely, GALs in any of the WW95 runs have ISMs with abundances similar to observed ones. However, they do not show the gradient reported from observations of Galactic and extragalactic HII regions (e.g., Garnett et al. 1995; Kennicutt and Garnett 1996; Kobulnicky and Skillman 1996), although the simulated abundances extend only in the range  $-3.8 < \log(\text{O/H}) < -3.2$ . The simulated mean values are lower than the observed ones but it has to be recalled that we are not including PNe yields that are thought to be important contributors of C (and N).

Observations of (N/O) in HII regions show that this ratio increases with (O/H) (e.g., Pagel 1992). A gradient in the secondary element is actually predicted by the Simple Model, although the steepness of the predicted relation is much larger than that actually observed in HII regions. There are several hypothesis that may explain the origin of these differences (Pagel 1997). We estimate this relation for GALs in WW95 runs. As shown in Fig.12, the simulated ISMs have abundances that are in good agreement with observations. However, we only find GALs with  $12+ \log(\text{O/H}) < 8.5$ , while the observed gradient in HII regions is  $12+ \log(\text{O/H}) > 8.5$ . We do not find GALs with average ISM metallicity corresponding to solar abundances, neither extremely low metallicity IZW18 type objects. It should be considered, however, that only massive GALs are analysed in the simulations.

Another important observational correlation is that between  $12+ \log(\text{O/H})$  and the gas fraction estimated for irregular and blue compact galaxies (e.g., Axon et al. 1998). This relation can be used to assess the metal content of the ISMs in relation to the left-over gas mass of the corresponding GALs. In Fig.13, we plot  $12+ \log(\text{O/H})$  versus

**Table 4.** Mean  $Z_{\text{star}}$  and  $Z_{\text{gas}}$  values of GALs

	S1	S2	S3	S4	S5	S6	S7
$\langle Z_{\text{gas}}/Z_{\odot} \rangle$	$0.45 \pm 0.11$	$0.21 \pm 0.06$	$0.29 \pm 0.14$	$0.18 \pm 0.06$	$0.21 \pm 0.06$	$0.22 \pm 0.06$	$0.27 \pm 0.10$
$\langle Z_{\text{star}}/Z_{\odot} \rangle$	$0.43 \pm 0.06$	$0.26 \pm 0.05$	$0.44 \pm 0.15$	$0.25 \pm 0.05$	$0.31 \pm 0.06$	$0.24 \pm 0.04$	$0.26 \pm 0.06$

$\log (M_{\text{bar}}/M_{\text{gas}})$  for the ISM in the simulated GALs ( $M_{\text{bar}}$  and  $M_{\text{gas}}$  are the total baryonic and gaseous mass within  $2R_{\text{opt}}$ , respectively). Observations taken from Pagel (1997) have been included for comparison. The estimated abundance ratios in the models are consistent with observations. It is notable that the observed relation is well reproduced in the sense that objects with a lower gas fraction tend to have larger metallicities without the need to introduce other physical mechanisms such as SN energy injection effects to the ISM. The Simple Model predicts a decrease of the metallicity with the gas richness of the system but it fails to correctly reproduce the observational relation.

## 5 CONCLUSIONS

We have implemented a chemical model in a SPH cosmological code. First results are reported together with the assessment of the effects of model parameters and numerical resolution. It is found that the major problem introduced by a low numerical resolution is the artificial smoothing of the chemical properties of the objects. However if a minimum number of baryonic particles is imposed, then average values can be considered reliable.

The mean metallicity is found nearly independent of the total stellar mass of the system indicating that the effects of mergers, interactions and gas infall on the mass distribution and metal mixing are very significant. We find correlations between the stellar mass  $M_{\text{star}}$  and the virial and optical circular velocities ( $V_{\text{vir}}$ ,  $V_{\text{opt}}$ ). However, the correlation with  $V_{\text{opt}}$  is significantly tighter, consistent with the Tully-Fisher relation. Nevertheless, the global metallicity of GALs,  $Z_{\text{star}}$  shows no dependence on  $V_{\text{opt}}$ , in spite of the fact that these GALs satisfy the Tully-Fisher relation and shows a strong correlation between the global metallicity of their stars and gas components with the left-over gas fraction of the systems. We only find a significant correlation between the global GALs metallicity of both stars and gas with the left-over gas fraction of the systems.

An analysis of the GALs assuming they have behaved according to the one-zone Simple Model show important differences with the results of the numerical simulations. The slope of  $Z_{\text{star}}/Z_{\odot}$  versus  $M_{\text{gas}}/M_{\text{bar}}$  and the systematic increase of stellar metallicity as a function of the stellar mass formed in the Simple Model contrasts with the behaviour of the numerical simulations. We find that the Simple Model overestimates the metallicity of the galactic gaseous components if it is constrained to match the stellar chemical content. According to the Simple Model, the global metallicity of a system continuously increases with the stellar mass in disagreement with the results found for the simulated GALs that show higher metallicities for intermediate mass objects.

We find that the star formation efficiency, SN model parameters and the nucleosynthesis yields significantly affect the chemical properties of the GALs. In those models

where the SF process is gradual the mean stellar and gaseous metallicities are similar.

The observed abundance ratios for primary and secondary elements in Galactic and extragalactic HII regions are naturally obtained. However, the ranges of the simulated global metallicities are smaller than the observed ones. Also, the relation between the (O/H) and gas fraction obtained in the numerical simulations is consistent with the observational results.

The suitable agreement between the models and the observations for these relations suggests that hierarchical clustering scenarios are able to reproduce the chemical properties of galaxies. This is a very encouraging fact taken into account that galactic objects formed by the accretion and mergers of substructure. Violent events are common and ubiquitous, and can affect the dynamical evolution of the matter, regulating the SF and chemical evolution in galactic objects.

We intend to improve this chemical model in the future by allowing the gaseous component to cool according to its metallicity, and a further study of the mixing process of chemical element in the ISM. It is also under study a more efficient decoupling mechanism between stars and gas that could shorten the period of hybrid state of a baryonic particle. Finally, energy feedback remains an open question that we hope to address in a future work.

## ACKNOWLEDGMENTS

We thank S. Woosley for kindly providing the yield tables and L. Portinari for clarifying some aspects of their nucleosynthesis model. We also thank M. Abadi for useful discussions. P. Tissera is grateful to C. Chiappini for introductory discussion in chemical evolution during the 1999 Aspen Summer Workshop. The authors thank the hospitality of the Observatorio Astronómico Centroamericano de Suyapa while finishing the writing of this paper. P. Tissera is grateful to the Observatorio Astronómico de Córdoba and the research group IATE for allowing the use of their computational facilities. M. Mosconi thanks IAFE for their hospitality during the preparation of this work. This work has been partially supported by CONICET, CONICOR, SECYT and Fundación Antorchas.

## REFERENCES

- Axon D. J., Staveley-Smith L., Fosbury R. A. E., Danziger J., Boksenberg A., Davies R. D., 1988, MNRAS, 231, 1077
- Barnes J., Hernquist L., 1996, ApJ, 471, 115
- Bottema A. H., 1992, A & A, 328, 517
- Burkert A., Truran J. W., Hensler G., 1992, ApJ, 391, 651
- Blumenthal G. R., Faber S. M., Flores R. A., Primack J. P., 1986 ApJ, 301, 27
- Chiappini C., Matteucci F., Gratton R., 1997, ApJ, 477, 765

- Cora S. A., Tissera P. B., Lambas D. G., Mosconi M. B., 2000, *Proceeding of 'Galaxy Disks and Disk Galaxies'* Rome, 12-16 June, 2000.
- Cowie L. L., Songaila A., Hu E. M., Cohen J. G., 1996, *ApJ*, 112, 839
- Courteau S., de Jong R. S., Broeils, A. H., 1996, *ApJ*, 457, L73
- Dalgarno A., McCray R.A., 1972, *AR&AA*, 10, 375
- Dekel A., Silk J., 1986, *ApJ*, 303, 39
- Domínguez-Tenreiro, R., Tissera P., Sáiz A., 1998, *ApJ*, 508, L123
- Edvardsson B., Andersen J., Gustafsson B., Lambert D. L., Nissen P. E. Tomkin, J., 1993, *A&AS*, 274, 101
- Ellis R. S., Colless M., Broadhurst T., Heyl J., Glazebrook K., 1996, *MN*, 280, 235
- Ferrini F., Matteucci F., Pardi C., Peuco U., 1992, *ApJ*, 387, 138
- Garnett D. R., Sillman E. D., Dufour R. J., Peimbert M., Torres-Peimbert S., Shields G. A., Terlevich R. J., Terlevich E., 1995, *ApJ*, 443, 64
- Gratton R., Cannetta E., Matteucci F., Sneden C., 1996, *Morrison H., Sanajedini A., eds., Formation of the Galactic Halo, Inside out*, vol.92, p.307
- Greggio L., 1996, Kunth D., Guiderdoni B., Heydari-Malayeri M., and Thuan T., eds., *The 11th IAP Astrophysics Meeting: The Interplay Between Massive Star Formation, the ISM and Galaxy Evolution*, p.89
- Katz N. 1992, *ApJ*, 391, 502
- Kennicutt R., Jr., Garnett D. R., 1996, *ApJ*, 456, 504
- Kobulnicky H. A., Skillman E. D., 1996, *ApJ*, 471, 211
- Kunth D., Ostlin G., 1999. To appear in *ARA&A*
- Larson R., 1975, *MNRAS*, 173, 671
- Larson R., 1976, *MNRAS*, 176, 31
- Lilly S. J., Tiesse L., Hammer F., Crampton D., Le Fevre O., 1995, *ApJ*, 441, 18
- Lu L., Sargent L. W., Barlow T., Churchill C., Vogt S., 1996, *ApJS*, 107, 475
- Madau M. P., 1995, *ApJ*, 441, 18
- Madau P., Ferguson H., Dickinson M., Giavalisco M., Steidel C., Fruchter A., 1996, *MNRAS*, 283, 1388
- Matteucci F., Franco P., 1989, *MNRAS*, 239, 885
- Metzler C. A., Evrard A. E., 1994, *ApJ*, 437, 564
- Mihos J. C., Hernquist L., 1996, *ApJ*, 464, 641
- Navarro J.F., White S.D.M. 1994, *MNRAS*, 267, 401
- Navarro J. F., Steinmetz M., 2000, *astro-ph/0003384*
- Pagel B. E. J., 1992., Alloin D., Stansiska G., eds., *The Feedback of Chemical Evolution on the Stellar Content of Galaxies*, p.87
- Pagel B. E. J., 1997, *Nucleosynthesis and Chemical Evolution of Galaxies*, Cambridge University Press, United Kingdom
- Pettini M., Smith L., King D., Hunstead R., 1997, *ApJ*, 998, 665
- Portinari L., Chiosi C., Bressan A., 1998, *A&AS*, 334, 505 (P98)
- Raiteri C. M., Villata M., Navarro J. F., 1996, *A&AS*, 315, 105
- Renzini A., 1998, D'Odorico, Fontana A., Giallongo E., eds., *ASP Conference Series, The Young Universe: Galaxy Formation and Evolution at Intermediate and High Redshift*, vol.146, p.298
- Rhee M. H., 1996, Ph.D. thesis, University of Groningen
- Rocha-Pinto H. J., Maciel W. J., Flynn C., 2000, *A&A*, submitted (*astro-ph/0001383*)
- Samland, M., Hensler, G., Theis, CH., 1997, *ApJ*, 476, 544
- Schmidt M., 1963, *ApJ*, 137, 758
- Springel, V., 2000, *MNRAS*, 312, 859
- Steidel C. C., Hamilton D., 1992, *AJ*, 104, 941
- Steidel C. C., Adelberger K. L., Giavalisco M., Dickinson M., Pettini M., 1998, *ApJ*, submitted (*astro-ph/9811399*)
- Steinmetz, M., & Müller, E. 1994, *A&A*, 281, L97
- Steinmetz, M., & Müller, E. 1995, *MNRAS*, 276, 549
- Tenorio-Tagle G., Sergey A. S., Kunth D., Terlevich E., Roberto Terlevich R., 1999, *MNRAS*, in press
- Thielemann F. K., Nomoto K., Hashimoto M., 1993, Prantzos N., Vangoni-Flam E., Cassé N., eds., *Origin and Evolution of the Elements*, p.299
- Thomas P. A. Couchman H. M. P., 1992, *MNRAS*, 257, 11
- Tinsley B. M., 1980, *Fundamental of Cosmic Physics*, vol.5, p.287
- Tissera P. B., 2000, *ApJ*, 534, 636
- Tissera P. B., Domínguez-Tenreiro R., 1998, *MNRAS*, 297, 177
- Tissera P.B., Lambas D.G., Abadi M.G., 1997, *MNRAS*, 286, 384
- Tissera P. B., Mosconi M. B., Cora S. A., Lambas D. G., 2000, in preparation
- Tosi M., 1996, *From Stars to Galaxies: The Impact of Stellar Physics on Galaxy Evolution*, ASP, Conf.Ser., vol.198, p.229
- van den Bergh S., 1991, Woosley S. E., ed., *The Tenth Santa Cruz Workshop in Astronomy and Astrophysics: Supernovae*, p.711
- van den Bergh S., 1962, *A&AS*, 67, 486
- White S.D.M., Frenk C.S. 1991, *ApJ*, 379, 25
- White S. D. M., 1981, *MNRAS*, 191, 1
- Woosley S. E., Weaver T. A., 1995, *ApJS*, 101, 181

**Figure 3.**  $[\text{O}/\text{Fe}]$  vs.  $[\text{Fe}/\text{H}]$  for experiments E4, E5 and E6 where the relative ratio of SNII/SNI ( $\Theta_{\text{SN}}$ ), the star formation efficiency ( $C$ ) and the nucleosynthesis yields have been changed with respect to E1. Time  $t$  is given in units of  $10^{10}$  yr.

**Figure 4.** Comparison of the  $[\text{C}/\text{Fe}]$  vs.  $[\text{Fe}/\text{H}]$  relation for experiments E1: WW95 and E6: P98, yields. Time  $t$  is given in units of  $10^{10}$  yr.

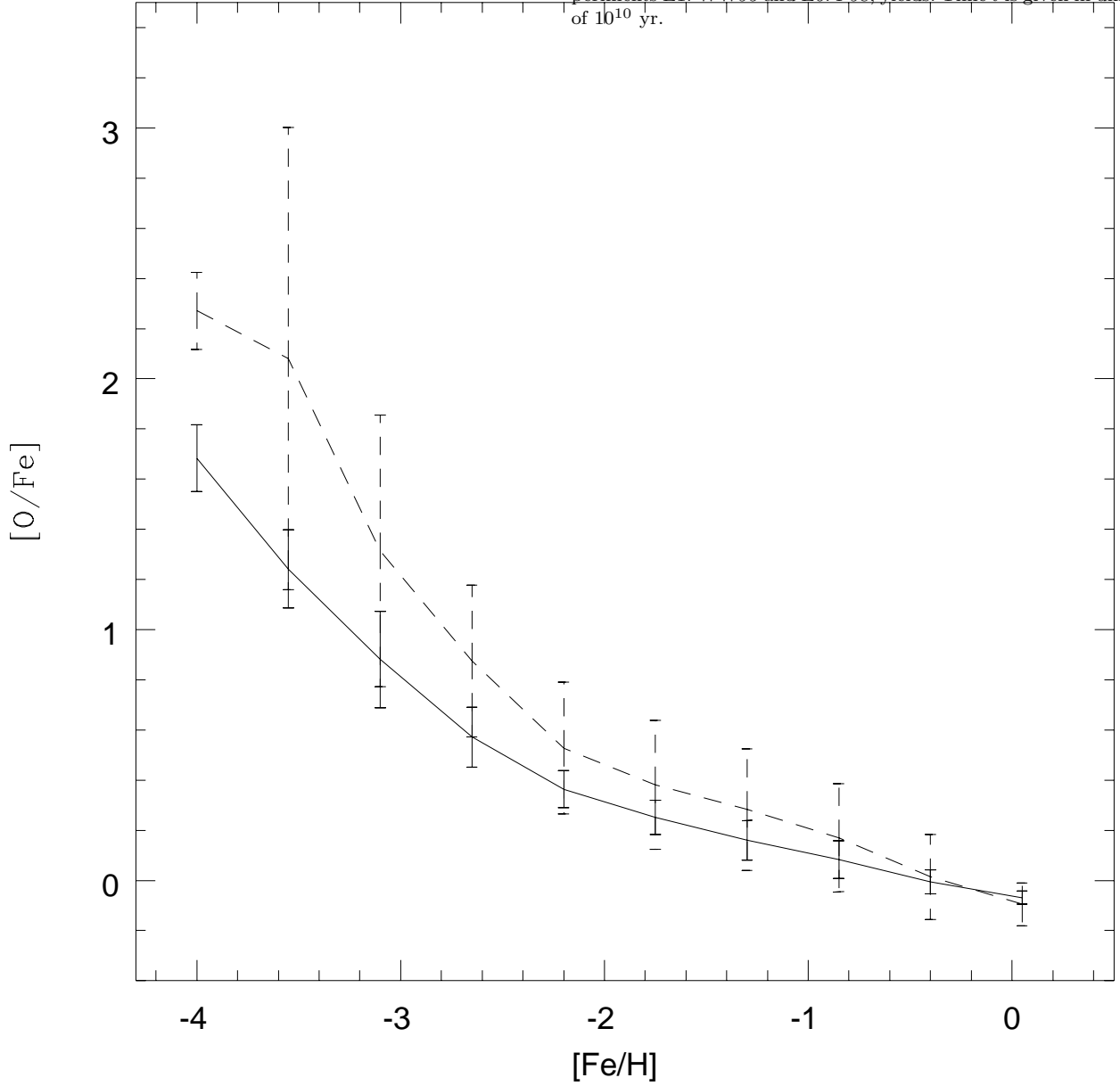


**Figure 1.** Comparison of the  $[\text{O}/\text{Fe}]$  versus  $[\text{Fe}/\text{H}]$  relation obtained from the low (solid line) and high resolution tests (dashed lines).

**Figure 2.**  $[\text{O}/\text{Fe}]$  vs.  $[\text{Fe}/\text{H}]$  for experiments E1, E2 and E3 where the life-time of binary systems has been varied:  $10^8$  yr,  $4 \times 10^8$  yr and  $10^9$  yr, respectively. Time  $t$  is given in units of  $10^{10}$  yr.

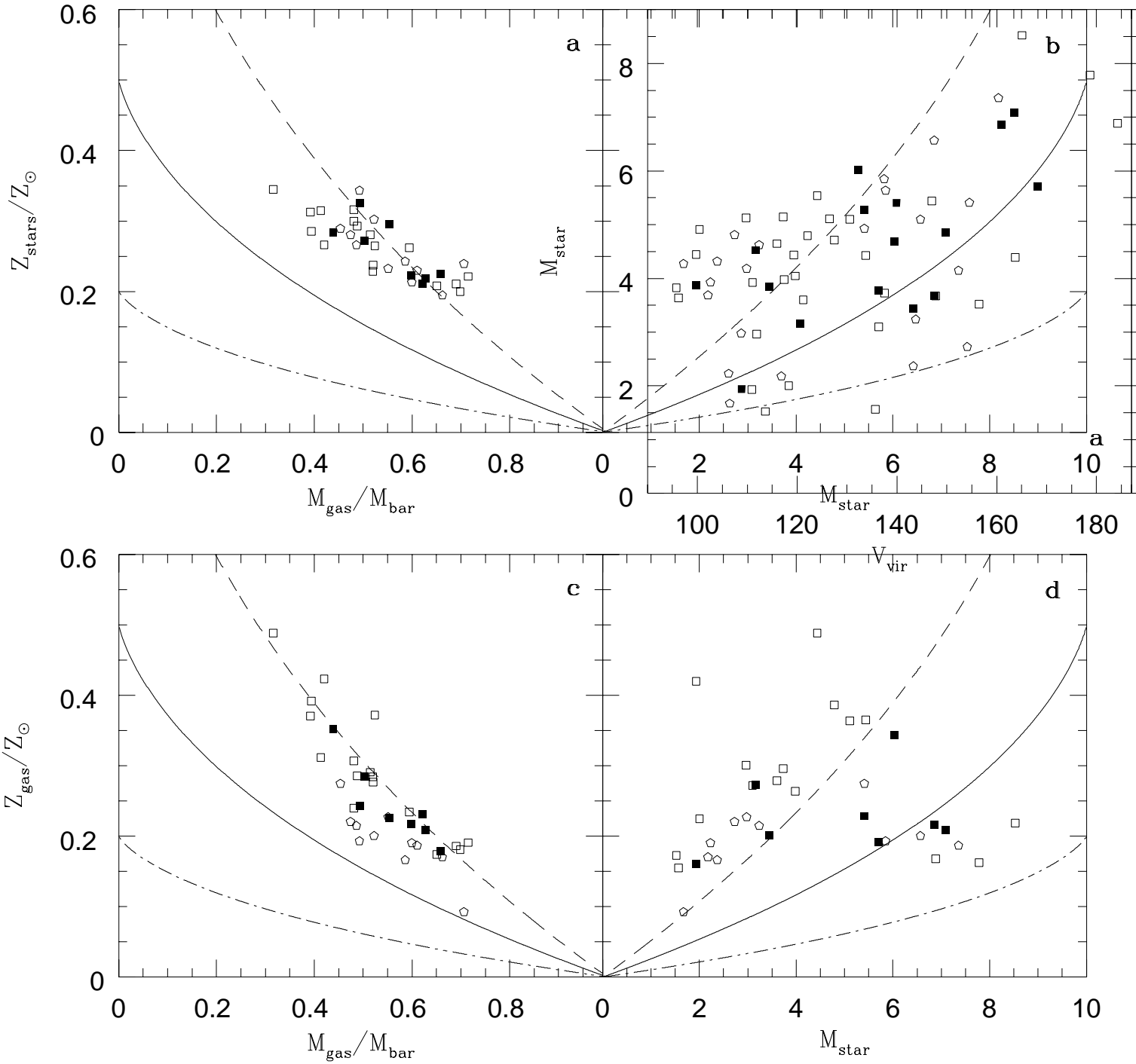


**Figure 5.** Global metallicities of the stellar population and gas component in GALs as a function of their gas fraction,  $M_{\text{gas}}/M_{\text{bar}}$ , (a,c), and their total stellar mass,  $M_{\text{star}}$ , (b,d) in simulations S2 (open pentagons), S6 (filled squares) and S7 (open squares). Lines represent the relations given by the Simple Model for  $0.2Z_{\odot}$  (dotted-dashed lines),  $0.5Z_{\odot}$  (solid lines) and  $Z_{\odot}$  (dashed lines).  $M_{\text{star}}$  is given in units of  $10^{10} M_{\odot}$ .

**Figure 6.** The total stellar mass of GALs ( $M_{\text{star}}$ ) as a function of a) the virial velocity ( $V_{\text{vir}}$ ) and b) the optical velocity ( $V_{\text{opt}}$ ) for the same GALs shown in Fig.5. Velocities are given in  $\text{km s}^{-1}$  and  $M_{\text{star}}$  is given in units of  $10^{10} M_{\odot}$ .

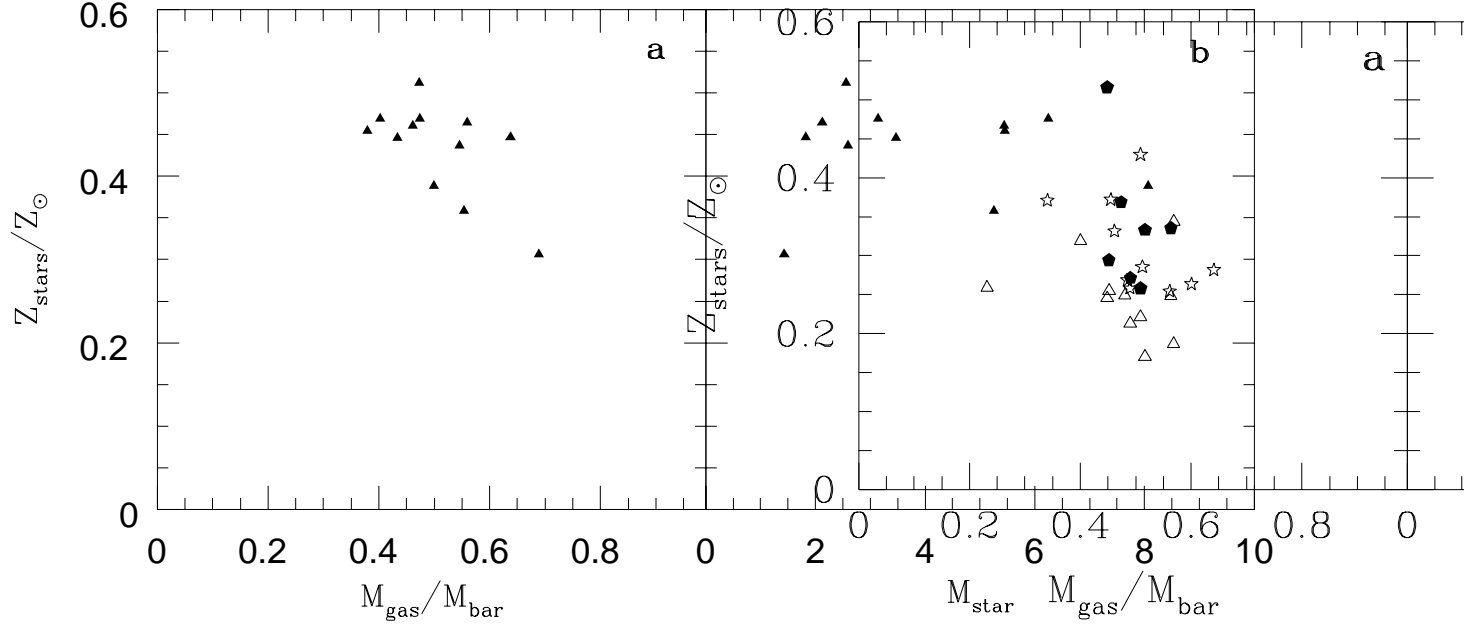


**Figure 7.** Global metallicities of the stellar populations in GALs ( $Z_{\text{star}}/Z_{\odot}$ ) in simulation S1 (P98) as a function of a) the gas fraction ( $M_{\text{gas}}/M_{\text{bar}}$ ), and b) the total stellar mass ( $M_{\text{star}}$ ) of GALs.  $M_{\text{star}}$  is given in units of  $10^{10} M_{\odot}$ .

**Figure 8.** Global metallicities of the stellar populations ( $Z_{\text{star}}/Z_{\odot}$ ) as a function of a) the gas fraction ( $M_{\text{gas}}/M_{\text{bar}}$ ), and b) the total stellar mass ( $M_{\text{star}}$ ) of GALs in simulations S3 (filled pentagons), S4 (open triangles) and S5 (open stars).  $M_{\text{star}}$  is given in units of  $10^{10} M_{\odot}$ .

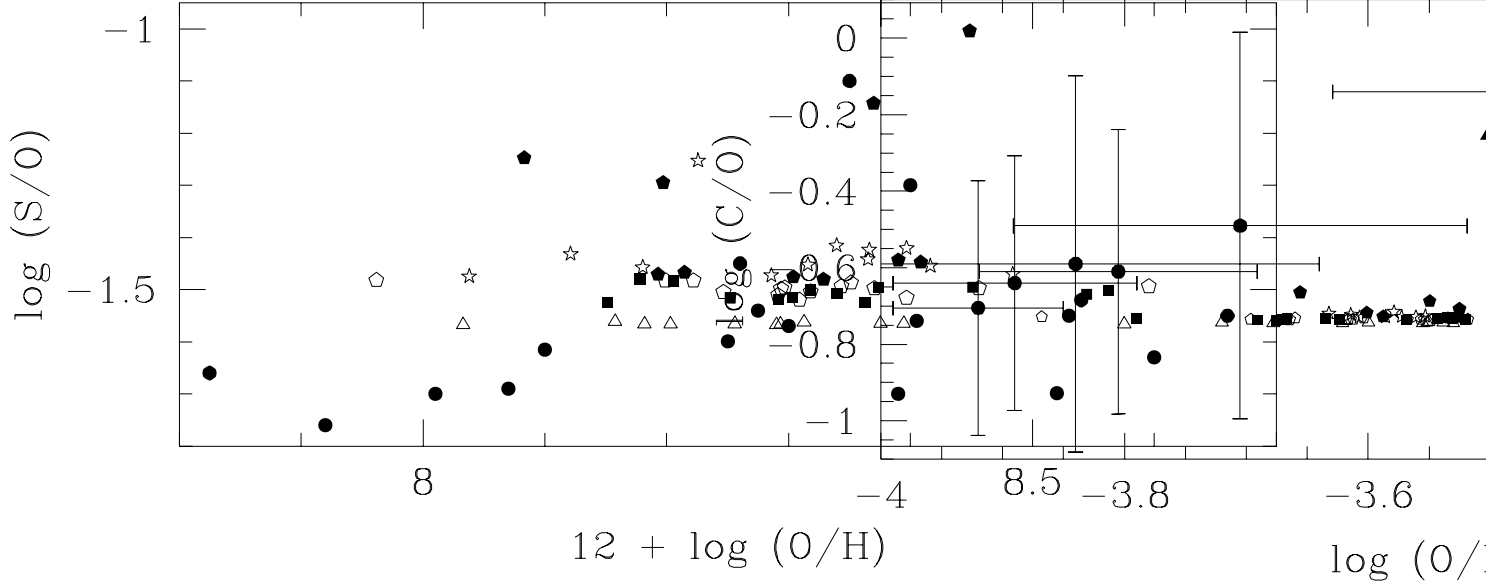


**Figure 9.** (S/O) versus (O/H) for the ISM of GALs in simulations S2, S3, S4 and S5 (see Fig.5 and 8 for feature code). Observations of HII regions have been included (small filled circles).

**Figure 10.** (C/O) versus (O/H) for the ISM of GALs in simulations S2, S3, S4 and S5 (see Fig.5 and 8 for feature code). GALs in S1 (filled triangles) have been included. Observations of HII regions have been included (small filled circles).



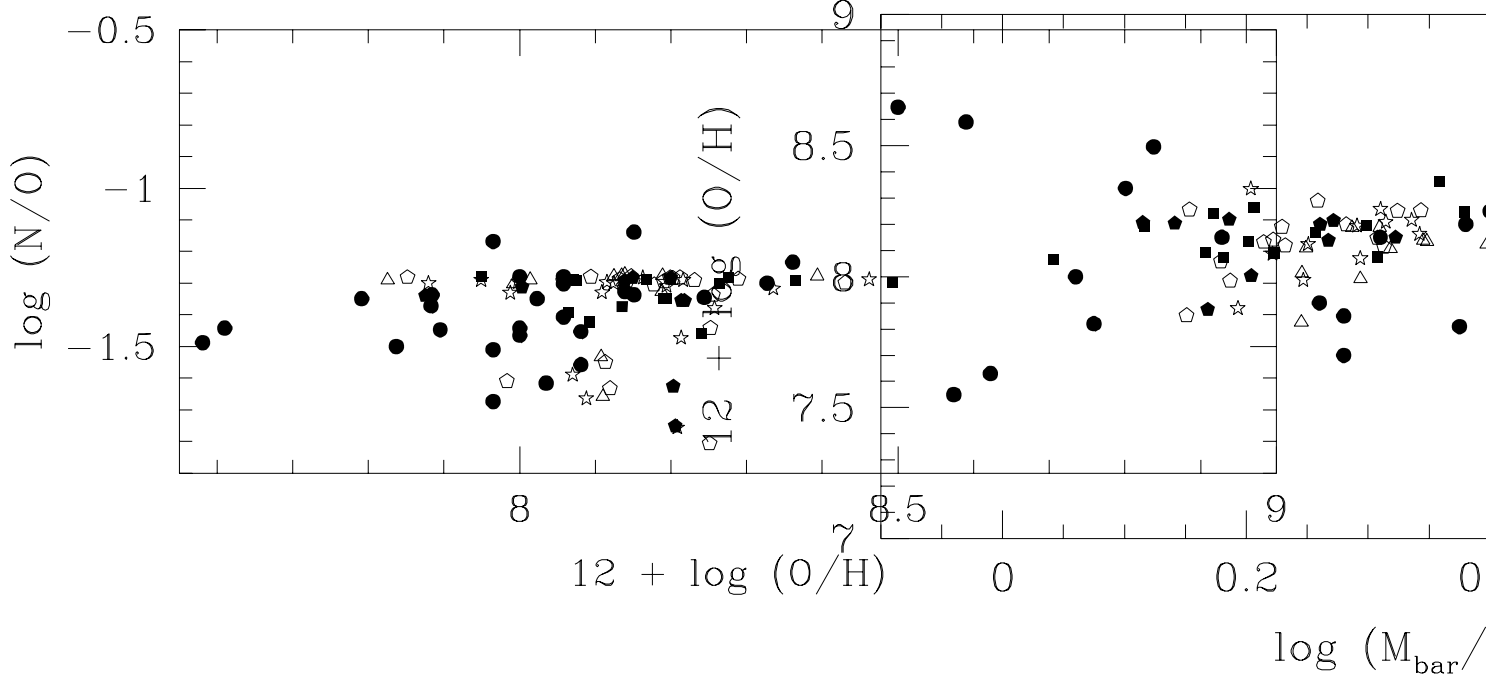


**Figure 11.** (N/O) versus (O/H) for the ISM of the GALs shown in Fig.9. Observations of HII regions have been included (small filled circles).

**Figure 12.** Logarithm of the oxygen abundances versus the logarithm of their gas fraction for the same GALs shown in Fig.9. Observations of HII regions in blue compact and irregular galaxies from Pagel (1997) have been included (small filled circles).

This figure "figure2test.jpg" is available in "jpg" format from:

<http://arxiv.org/ps/astro-ph/0007074v1>

This figure "figure3test.jpg" is available in "jpg" format from:

<http://arxiv.org/ps/astro-ph/0007074v1>

This figure "figure4test.jpg" is available in "jpg" format from:

<http://arxiv.org/ps/astro-ph/0007074v1>